Applied Ocean Research 109 (2021) 102564

Contents lists available at ScienceDirect

Applied Ocean Research

journal homepage: www.elsevier.com/locate/apor

Sliding mode control unified with the uncertainty and disturbance estimator for dynamically positioned vessels subjected to uncertainties and unknown disturbances

Chaodong Hu [a], Defeng Wu [a,b,*], Yuxiang Liao [a], Xin Hu [c]

[a] School of Marine Engineering, Jimei University, Xiamen 361021, PR China
[b] Fujian Provincial Key Laboratory of Naval Architecture and Ocean Engineering, Xiamen 361021, PR China
[c] School of Mathematics and Statistics Science, Ludong University, Yantai 264025, PR China

ARTICLE INFO

Keywords:
Uncertainty and disturbance estimator
Sliding mode control
Dynamic positioning vessel
Unknown mode parameters
Observer

ABSTRACT

When considering the characteristics of a dynamic positioning (DP) vessel involving uncertain modelling and unknown disturbances, the vessel control problem becomes a mismatched nonlinear control issue. To resolve this issue, this paper proposes a control method based on the sliding mode control (SMC) and the uncertainty and disturbance estimator (UDE). The total disturbance in the DP vessel is determined using the UDE, whereas the trajectory tracking function of the vessel is achieved via SMC. Moreover, the estimation error in the UDE and the tracking error of the SMC were found to converge based on the Lyapunov theory. The effectiveness of the proposed control strategy was verified via simulations. A comparative study involving the conventional SMC was also conducted, revealing that the proposed SMC unified with the UDE yielded a considerably superior performance.

1. Introduction

A majority of the Earth's surface is covered by oceans. Given that land resources are limited and rapidly declining, humans have devoted increasing efforts toward the extraction and utilisation of ocean resources. Unmanned equipment plays a vital role in extracting such resources from the deep sea or other similar regions where manual exploration is challenging and even dangerous. Owing to developments in automatic control techniques and other similar approaches, vessels equipped with dynamic positioning (DP) systems are being deployed to facilitate the utilisation of marine resources. Such vessels with DP are fully actuated vessels that can be operated conveniently, even in deep sea areas. These vessels can realise positioning and heading control by means of their propellers, while performing dynamic positioning and trajectory tracking operations (Wu et al., 2017; Wu et al., 2021). Generally, the use of a DP vessel enhances safety, decreases personnel costs and enables operations under harsh conditions.

The control strategy employed in DP vessels is of great significance. Consequently, several studies have focused on proposing control strategies for DP. For instance, an adaptive fuzzy proportional integral derivative (PID) controller based on a segmented PID controller was proposed by Wang et al. (Wang et al., 2019) for application in DP systems. Moreover, a univariate method for performance adjustments and online robustness improvements was proposed in (Verma and Padhy, 2020). They focused on online adjustments and the robustness of the PID controller. Marine environments can be highly complex, making it significantly difficult to identify interference boundaries of the external environment. Recently, the active disturbance rejection controller (ADRC) has attracted considerable attention as an effective control technology (Ma et al., 2018; Wu and Li, 2018). The robustness of nonlinear systems can be enhanced using the ADRC, thereby enabling the control of such systems, including vessels (An et al., 2019). However, the performances of these previous methods prove to be unsatisfactory when the system involves unknown environmental disturbances and modelling uncertainties.

Sliding mode control (SMC) offers robustness against unknown environmental disturbances; hence, it is widely used in the control of nonlinear systems such as vessels. Fahimi proposed the application of SMC to an under-actuated vessel (Fahimi, 2007), whereby the performance of the SMC under environmental interference was determined via simulations. A non-singular terminal SMC method was proposed by Hu et al. (Hu et al., 2020). Such studies have led to SMC advancements in

* Corresponding author.
E-mail address: defeng@jmu.edu.cn (D. Wu).

https://doi.org/10.1016/j.apor.2021.102564
Received 17 September 2020; Received in revised form 3 December 2020; Accepted 3 February 2021
Available online 24 February 2021

the field of maritime navigation and control. Inspired by dynamic surface control, a low-pass filter was proposed by Wang et al., 2014 with the aim of preventing the 'explosion problem' in the conventional reverse thrust design. The hierarchical sliding mode and backstepping control routines were combined by Hadi and Hamid, 2018, thereby realising trajectory tracking control of a wheeled mobile robot. Moreover, an adaptive SMC suitable for maritime navigation was proposed by Kim et al. (Kim and Hong, 2019), and experiments were conducted in the presence of interference. A finite-time control method based on a high-order sliding mode observer was proposed by Besant et al. (Basin et al., 2017); rapid responses in missile control were achieved using this method. The finite-time extended state observer-based formation control for marine surface vehicles subjected to environmental disturbances and input saturation was proposed by Fu et al. (Fu. and Yu, 2018). Chen et al. proposed adaptive sliding mode control based on neural network, which improves the control accuracy of remote robots in unknown environments (Chen et al., Feb. 2020; Chen et al., 2020). Yu et al. (Yu. et al., 2005) proposed a continuous finite-time control with a terminal sliding mode and employed it in the control of robot manipulators. Furthermore, SMC was employed by Chen et al. (2016) for multi-vessel cooperative control. A sliding mode tracking controller was designed to solve the consistency problem of an under-actuated vessel; this controller achieved excellent performance in the cooperative control of an under-actuated vessel. Generally, SMC has a variable structure and exhibits excellent resilience to external environmental disturbances. However, due to the influence of modelling uncertainty, several problems such as chattering occur in the control system.

In recent years, the control of unknown systems has gained widespread research attention, and several effective methods for the compensation of system uncertainties have been proposed. A robust control based on the UDE for a class of non-affine nonlinear systems was proposed by Ren et al. (Ren et al., 2015). This class of systems was highly general, covering a wide range of nonlinear systems. Aharon et al. (Aharon. et al., 2011) proposed a UDE filter design methodology addressing the constraint of limited bandwidth. Based on stability conditions, a system design methodology based on a reference model involving pole placement and controllable classical transformation was proposed by Tian et al. (Tian et al., 2019). Moreover, a robust control strategy for uncertain nonlinear systems with input/output delays was proposed by Sanz et al. (Sanz et al., 2017). This control strategy was verified via experiments involving a quadrotor. Compared with SMC, the UDE has fewer applications in the field of maritime navigation and control. The amplitude of interference can be considered using other typical interference observer-based control methods; however, UDE-based control only requires bandwidth information of the interference.

SMC offers several advantages for nonlinear systems, such as robustness, fast responses, and ease of implementation (Liu et al., 2014). Moreover, the UDE does not require model accuracy, making it relatively more applicable (Deepika. et al., 2018; Gadelovits et al., 2017). Considering the simplicity of implementation and the accuracy of control, a control method combining UDE with the conventional SMC is proposed herein. The primary highlights of this work are listed as follows:

(1) The SMC of the DP ship is adopted to control the position and heading of the ship during the voyage. UDE is employed to estimate the uncertainty of modeling in the dynamic positioning vessel and the interference of the external marine environment.
(2) The actual torque limits of the thrusters are considered. Compared with the traditional SMC, the control accuracy of the proposed SMC unified with the UDE is significantly enhanced.
(3) In the proposed control strategy, the input chattering in traditional SMC is suppressed due to the introduction of UDE.

The remainder of this paper is organised as follows. The mathematical model and control objectives of DP vessel motion are discussed in Section 2. The proposed SMC unified with the UDE is introduced in Section 3. Section 4 presents the verification of this proposed strategy via simulations. Finally, conclusions of this work are presented in Section 5.

Notations: For a better understanding of the formulas used in subsequent sections, consistently used symbols are explained in Table 1. The remaining parameters are explained when they appear in the discussions.

2. Mathematical model for DP vessel

The mathematical model of a DP vessel includes the kinematic model and the dynamic model.

2.1. Kinematic model of the DP vessel

For a ship with DPS, it usually moves on the sea at a relatively low speed (Wu et al., 2016; Huang et al., 2021). The actual movement of a DP vessel is more complicated, typically involving six degrees of freedom as the robotic manipulator (Zhang et al., 2018). However, for the trajectory tracking control of low-speed surface vessels, only three degrees of freedom are generally considered: surge, sway, and yaw (Fossen and Strand, 1999). The movement of a three-degree-of-freedom fully actuated vessel is depicted in Fig. 1; in the figure, $o_1 - x_1y_1z_1$ is an inertial coordinate system fixed to the surface of the earth, the direction indicated by o_1x_1 is true north, the direction indicated by o_1y_1 is true east, and the direction indicated by o_1z_1 is geocentric. $o - xyz$ is the onboard system containing the origin of the DP vessel. The origin o is the centre point where the bow of the DP vessel is connected to the stern; ox corresponds to the bow along the centreline of the vessel, oy denotes the starboard side of the vessel, and oz refers to the centre of the earth. When the origins of these two coordinate systems coincide and the heading angle is ϕ, these coordinate systems satisfy the following conversion relationship:

$$\begin{bmatrix} x \\ y \end{bmatrix} = \begin{bmatrix} \cos\phi & \sin\phi \\ -\sin\phi & \cos\phi \end{bmatrix} \begin{bmatrix} x_1 \\ y_1 \end{bmatrix} \tag{1}$$

The kinematic model for a DP vessel can be expressed as Eq. (2):

$$\dot{\eta} = J(\phi)\upsilon \tag{2}$$

The parameter matrices $J(\phi)$ can be expressed as

$$J(\phi) = \begin{bmatrix} \cos\phi & -\sin\phi & 0 \\ \sin\phi & \cos\phi & 0 \\ 0 & 0 & 1 \end{bmatrix}$$

where the vector $\eta = [x \quad y \quad \phi]^T$ denotes the actual positions and heading angle in the earth-fixed frame, comprising the surge position x, sway position y, and heading angle ϕ. The vector $\upsilon = [u \quad v \quad r]^T$represents the actual speed of the vessel and the actual yaw

Table 1
Explanation of parameter symbols.

Notation	Description
η	Position and heading of the vessel
υ	Velocity of the vessel in all directions
$u = \tau$	Control input
e	Trajectory tracking error
ρ	Limit value of total uncertainty
$\prod$	Limit value of derivative of total uncertainty
$\vartheta(\eta, \upsilon)$	Total nominal component
$\wp(\eta, \upsilon, t)$	Total model uncertainty
$\widehat{\wp}(\eta, \upsilon, t)$	Estimated value of uncertainty

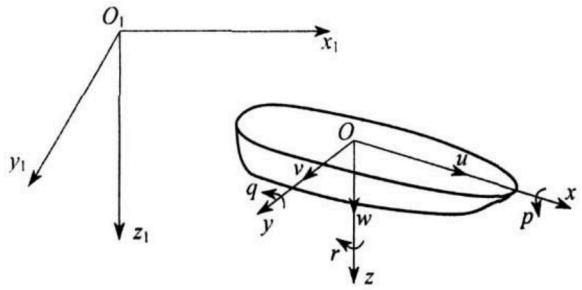

Fig. 1. Motion of the vessel in the inertial and onboard coordinate systems.

angular velocity in the inertial coordinate system; it comprises the surge velocity u, sway velocity v, and yaw rate r.

2.2. Dynamic model of the DP vessel

In the onboard coordinate system, the surge, sway, and yaw movements of the DP vessel can be described by the following expression:

$$M\dot{v} + C(v)v + Dv + f(\eta, v) = \tau + d \tag{3}$$

where the vector $\tau = [\tau_1 \quad \tau_2 \quad \tau_3]^T$ denotes the control input comprising the forward force τ_1, drift force τ_2, and turning force τ_3. The second input is the environmental disturbance vector d, which is an adverse effect. The vector $f(\eta, v) \in R^3$denotes model uncertainties. Where M is a matrix composed of ship weight inertia and hydrodynamic additional inertia, $C(v)$ is the Coriolis matrix and D is the linear hydrodynamic damping parameter matrix.

Based on Eqs. (2) and (3), the model of the DP vessel system can be expressed as

$$\begin{aligned}\ddot{\eta} &= \dot{J}(\phi)v + J(\phi)\dot{v} \\ &= \dot{J}(\phi)v + J(\phi)M^{-1}\tau + J(\phi)M^{-1}[d - C(v)v - Dv - f(\eta, v)]\end{aligned} \tag{4}$$

Let $x_1 = \eta, x_2 = \dot{\eta}$. Therefore, the model for the DP vessel can be rewritten as

$$\dot{x}_1 = x_2 \tag{5}$$

$$\begin{aligned}x_2 &= \dot{J}(\phi)v + J(\phi)M^{-1}\tau + J(\phi)M^{-1}[d - C(v)v - Dv - f(\eta, v)] \\ &= \Lambda\tau + \Lambda\Big(-C(v)v - Dv + \dot{J}(\phi)v + \Lambda(d - f(\eta, v))\Big) \\ &= \Lambda u + \vartheta(\eta, v) + \wp(\eta, v, t)\end{aligned} \tag{6}$$

where $u = \tau, \Lambda = J(\phi)M^{-1}, \vartheta(\eta, v) = \Lambda(-C(v)v - Dv + \dot{J}(\phi)v)$ denotes the total nominal component, and $\wp(\eta, v, t) = \Lambda(d - f(\eta, v))$ denotes the total uncertainty.

For better design the controller of vessel, the following two assumptions are proposed.

Assumption 1. The target trajectory of the DP vessel η_d is bounded and derivable. The first derivative of the target trajectory of the DP vessel $\dot{\eta}_d$ is bounded and exists.

Assumption 2. The value of total uncertainty is limited by $|\wp(\eta, v, t)| \leq \rho$, where ρ is an unknown constant. The value of the first derivative of $\wp(\eta, v, t)$ is bounded by $\| \dot{\wp}(\eta, v, t)\| \leq \Pi$, where Π is a known small positive constant.

3. Design of the SMC unified with the UDE

The control system for the DP vessel is presented in Fig. 2. The desired position and heading are input externally, with a slight difference from the actual position and heading of the vessel. Observers are usually used to deal with unknown disturbances (*Xie et al., 2021*). The UDE inputs the observed estimated total uncertainty into the controller, and the controller outputs the control torque required to ensure that the DP vessel travels along the desired trajectory.

In this system, the objective is to design a control u such that the DP vessel can be forced to follow the expected trajectory, despite the presence of uncertainties and disturbances represented by $\wp(\eta, v, t)$.

3.1. Design of the SMC

The design procedure for SMC is generally divided into two specific steps. The first step involves selecting the sliding mode surface and determining the equivalent control input, while the second step includes determining the reaching law that would guarantee the existence of the sliding mode surface (Aharon. et al., 2011; Yang et al., 2007):

$$x_d = \eta_d = [x_d \quad y_d \quad \phi_d]^T \tag{7}$$

The trajectory tracking error e and its derivative $\dot{e}$ are selected as

$$e = x_1 - x_d \tag{8}$$

$$\dot{e} = x_2 - \dot{x}_d \tag{9}$$

Simultaneously,the sliding mode surface is expressed as

$$\sigma = \dot{e} + \lambda e \tag{10}$$

where λ is an adjustable parameter.

Computing the time derivative of the sliding mode surface (10), we obtain

$$\dot{\sigma} = \ddot{e} + \lambda\dot{e} = \Lambda u + \vartheta(\eta, v) + \wp(\eta, v, t) - \ddot{x}_d + \lambda\dot{e} \tag{11}$$

The required control can be expressed as

$$u = u_n + u_s \tag{12}$$

where u_n is the nominal system control, and u_s refers to the compensation for uncertainty.

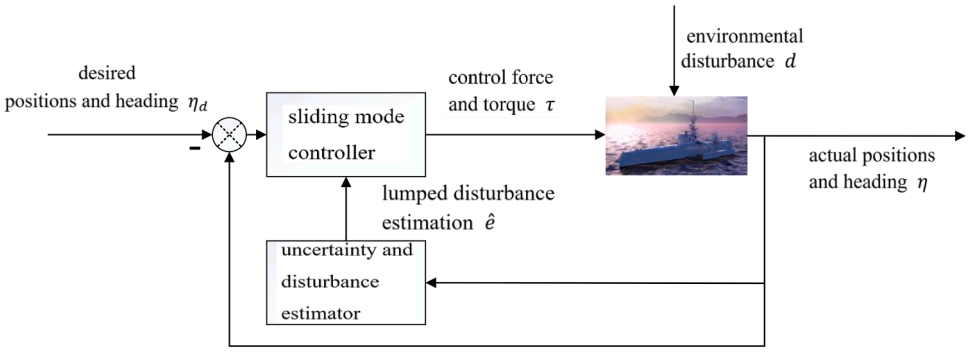

Fig. 2. Schematic of the vessel tracking control system.

$$u_s = -(\rho + \mathrm{K})\mathrm{sgn}(\sigma) \tag{13}$$

where ρ is presented in Assumption 2, and K is a sufficiently small positive constant.

Thus, the nominal system of vessel can be expressed as

$$\begin{cases} \dot{x}_1 = x_2 \\ \dot{x}_2 = \Lambda u_n + \vartheta(\eta, \upsilon) \end{cases} \tag{14}$$

Subsequently, the control u_n of the nominal system is calculated.

The following trajectory tracking error and its derivative can be rewritten as

$$\begin{cases} z_1 = \eta - \eta_d = x_1 - x_d \\ z_2 = \upsilon - \upsilon_d = \Lambda^{-1} M^{-1} \left(x_2 - \dot{x}_d \right) \end{cases} \tag{15}$$

In the eventual SMC, the existing condition of the sliding mode surface is determined using the Lyapunov function. To satisfy SMC existing condition, the control law of arrival is chosen as $\dot{\sigma} = -\varepsilon \mathrm{sgn}(\sigma)$, where ε is a known small positive constant.

On combining Eq. (11) and the control law, we obtain

$$\begin{aligned} u_n &= \Lambda^{-1} \left(\dot{J}(\phi)\upsilon - \vartheta(\eta, \upsilon) \right) + \Lambda^{-1} \ddot{x}_d - M\lambda J(\phi) z_2 - \varepsilon \mathrm{sgn}(\sigma) \\ &= \Lambda^{-1} \left(\ddot{x}_d - \vartheta(\eta, \upsilon) \right) + \xi(\eta, \upsilon, t) - \varepsilon \mathrm{sgn}(\sigma) \end{aligned} \tag{16}$$

For the sake of simplicity in the expressions, $J(\phi)M^{-1}\dot{J}(\phi)\upsilon - \delta(\eta, \upsilon, t)z_2$ is represented by $\xi(\eta, \upsilon, t)$, and $M\lambda J(\phi)$ is represented by $\delta(\eta, \upsilon, t)$.

The Lyapunov function for a three-degree-of-freedom fully actuated DP vessel control system is designed as

$$V = \frac{1}{2}(\sigma)^2 = \frac{1}{2}(\lambda z_1 + z_2)^2 \tag{17}$$

Computing the time derivative of Eq. (17), we obtain

$$\dot{V} = \lambda(z_1 + z_2) \left(\lambda J(\varphi) z_2 + \dot{z}_2 \right) \tag{18}$$

On combining the system Eq. (18) and the control law, Eq. (19) is obtained:

$$\lambda J(\phi) z_2 + \dot{z}_2 = -\varepsilon \mathrm{sgn}(\sigma) \tag{19}$$

The derivative of the Lyapunov function with respect to time is obtained as follows:

$$\dot{V} = \sigma\dot{\sigma} = -\sigma\varepsilon \mathrm{sgn}(\sigma) = -\varepsilon|\sigma| < 0 \tag{20}$$

Therefore, based on the Lyapunov function, the stability of the selected sliding surface can be verified.

Remark 1. The sliding mode surface is selected as $\sigma = \dot{e} + \lambda e$, due to which the two control quantities e and $\dot{e}$ of the system eventually tend to 0. $e = e(0)e^{-\lambda t}$and $\dot{e} = \dot{e}(0)e^{-\lambda t}$ can be determined as $s = 0$ and $\dot{e} + \lambda e = 0$. It is evident that the state quantity will eventually approach 0 at an exponential rate; when the sliding mode surface is designed, the larger the value of λ, the faster e and $\dot{e}$ tend to 0.

3.2. Design of the UDE

In order to design the UDE, the time-domain analysis of the DP vessel should be converted into a frequency-domain analysis, and the three-degree-of-freedom model of the DP vessel should be converted according to requirements.

$$\dot{x} = Ax + Bx + \Delta Ax + \Delta Bx + d(x, t) \tag{21}$$

where A and B are known constant matrices, x is a state vector, u is a control vector, ΔA and ΔB are system modelling uncertainty matrices, and $d(x, t)$ is an unknown disturbance.

Unknown disturbances and system modelling uncertainties are collectively termed as the total uncertainty:

$$E\tau_d = \Delta Ax + \Delta Bx + d(x, t) \tag{22}$$

where $E\tau_d$ are the total uncertainty.

The system equation for the DP vessel can be rewritten as

$$\begin{cases} y = Cx \\ \dot{x} = Ax + Bu + E\tau_d \end{cases} \tag{23}$$

The matrices A, B, C, and E in the formula can be expressed as follows: $A = \begin{bmatrix} 0 & I \\ -M^{-1}D & 0 \end{bmatrix}$, $B = \begin{bmatrix} 0 \\ M^{-1} \end{bmatrix}$, $C = [I \quad 0]$, and $E = \begin{bmatrix} 0 \\ M^{-1} \end{bmatrix}$.

The linear time invariant system is controlled by the UDE controller. In general models, DPS is often described as a nonlinear system. In order to adapt to the observer, the nonlinear system is converted to a linear system. In modern control theory, due to the existence of external input, the boundary between linear system and nonlinear system has been blurred. It can be proved that the behavior of a nonlinear system can be imitated by a linear control system.

The standard reference model is set to

$$\dot{x}_m = A_m x_m + B_m u_m \tag{24}$$

The control error of the standard model and the actual model is passed through the low-pass filter $G_f(s)$, and the final output is used as the total uncertainty of the SMC.

Therefore, an important aspect when designing the UDE is the filter. As a prerequisite, the bandwidth of the filter should be sufficiently wide to cover the frequency spectrum of the control amount u. According to (Sanz et al., 2017), the filter is designed using the principle of the internal model

$$G_f(s) = 1 - \frac{B_d(s)}{A_d(s)} \tag{25}$$

where $A_d(s)$ is an appropriate polynomial function of s, and $B_d(s)$ is determined by the external system model such that $G_f(s)$ remains stable; both $A_d(s)$ and $B_d(s)$ are limited.

The filter is designed as follows:

$$G_f(s) = \frac{1}{T_1 s^2 + T_2 s + 1} \tag{26}$$

where T_1 and T_2 is a constant, and the influence of bandwidth is considered in the design of $G_f(s)$. For a detailed design procedure, please refer to (Qin et al., 2018).

The effectiveness of the observer is derived in Theorem 1

Theorem 1. Considering that Assumption 2 holds, the uncertainty estimation $\widehat{\wp}(\eta, \upsilon, t)$ of the DP vessel based on the UDE can be approximated to the system uncertainty $\wp(\eta, \upsilon, t)$, and its uncertainty error $\widetilde{\wp}(\eta, \upsilon, t) = \wp(\eta, \upsilon, t) - \widehat{\wp}(\eta, \upsilon, t)$ will converge to 0.

Proof

When modelling uncertainty is considered, the sliding mode function is rewritten as

$$\sigma = \dot{e} + \lambda e + \wp(\eta, \upsilon, t) \tag{27}$$

The time derivative of Eq. (27) yields

$$\begin{aligned} \dot{\sigma} &= \ddot{e} + \lambda\dot{e} + \dot{\wp}(\eta, \upsilon, t) \\ &= \Lambda u + \vartheta(\eta, \upsilon) + \wp(\eta, \upsilon, t) - \ddot{x}_d + \lambda \left(x_2 - \dot{x}_d \right) + \dot{\wp}(\eta, \upsilon, t) \end{aligned} \tag{28}$$

Thus, Eq. (28) can be rewritten as

$$\wp(\eta, \upsilon, t) + \dot{\wp}(\eta, \upsilon, t) = \dot{\sigma} - \Lambda u + \vartheta(\eta, \upsilon) + \ddot{x}_d - \lambda\dot{e} = \Gamma(\eta, \upsilon, t) \tag{29}$$

Therefore,

$$\wp_{(s)}(\eta,\upsilon,t)=\Gamma_{(s)}(\eta,\upsilon,t)\frac{1}{s+1} \tag{30}$$

The total uncertainty is estimated as

$$\widehat{\wp}_{(s)}(\eta,\upsilon,t)=\Gamma_{(s)}(\eta,\upsilon,t)\frac{1}{s+1}G_f(s) \tag{31}$$

The estimated error of the total uncertainty is expressed as

$$\widetilde{\wp}_{(s)}(\eta,\upsilon,t)=\wp_{(s)}(\eta,\upsilon,t)-\widehat{\wp}_{(s)}(\eta,\upsilon,t)=\Gamma_{(s)}(\eta,\upsilon,t)\frac{1}{s+1}\left(1-G_f(s)\right) \tag{32}$$

where $\Gamma_{(s)}(\eta,\upsilon,t)$, $\wp_{(s)}(\eta,\upsilon,t)$, $\widehat{\wp}_{(s)}(\eta,\upsilon,t)$, and $\widetilde{\wp}_{(s)}(\eta,\upsilon,t)$ denote the Laplace transforms of $\Gamma(\eta,\upsilon,t)$, $\wp(\eta,\upsilon,t)$, $\widehat{\wp}(\eta,\upsilon,t)$, and $\widetilde{\Gamma}(\eta,\upsilon,t)$, respectively.

Based on the final value theorem, the following equation is obtained:

$$\begin{aligned}&\lim_{t\to\infty}\widetilde{\wp}_{(s)}(\eta,\upsilon,t)=\lim_{s\to0}s\widetilde{\wp}_{(s)}(\eta,\upsilon,t)\\&=\lim_{s\to0}\Gamma_{(s)}(\eta,\upsilon,t)\frac{s}{s+1}\left(1-G_f(s)\right)\\&=0\end{aligned} \tag{33}$$

From the abovementioned proof, it can be concluded that the observation error in the total uncertainty of the DP vessel, which was obtained via the UDE, gradually approaches 0. Therefore, Theorem 1 holds.

Remark 2. When designing the UDE, it should be noted that the amplitude boundary need not be known; only the frequency information (bandwidth) of the interfering signal is required. The frequency of the signal is more likely to be available or estimated; therefore, this aspect is a key difference between the UDE and many conventional interference observers.

3.3. Stability of the SMC unified with the UDE

The Lyapunov function is expressed as

$$V=\frac{1}{2}\sigma^T\sigma+\frac{1}{2}\partial\widetilde{\hbar}^T\widetilde{\hbar} \tag{34}$$

where $\widetilde{\hbar}=\hbar-\widehat{\hbar}$, ∂ is a positive adaptation gain, $\hbar$ is an unknown constant and $\widehat{\hbar}$ is the estimate of the boundary value $\hbar$.

According to Theorem 1, the total uncertainty $\wp(\eta,\upsilon,t)$ of the system can be replaced by the estimation $\widehat{\wp}(\eta,\upsilon,t)$ of the observer:

$$\wp(\eta,\upsilon,t)=\widehat{\wp}(\eta,\upsilon,t)+\delta \tag{35}$$

where δ is the error in disturbance approximation. It is assumed that this error is limited by the following factors:

$$\|\delta\|\le\hbar \tag{36}$$

According to (Shen et al., 2020), this assumption can be applied to the actual use of vessel.

The uncertainty estimate u_s is redesigned as

$$u_s=-(\widehat{\hbar}+\mathrm{K})\mathrm{sgn}(\sigma) \tag{37}$$

Therefore, the input u is rewritten as

$$u=u_n+u_s=\Lambda^{-1}\left(-\vartheta(\eta,\upsilon)+\ddot{x}_d\right)+\xi(\eta,\upsilon,t)-(\varepsilon+\widehat{\hbar}+\mathrm{K})\mathrm{sgn}(\sigma) \tag{38}$$

Under actual conditions, the output of dynamic positioning vessels is limited (Shen et al., 2020). The actual maximum driving force and torque output by the controller are limited, and Eq. (38) is rewritten as (39)

$$\begin{aligned}u&=u_n+u_s\\&=\begin{cases}\Lambda^{-1}\left(-\vartheta(\eta,\upsilon)+\ddot{x}_d\right)+\xi(\eta,\upsilon,t)-(\varepsilon+\widehat{\hbar}+\mathrm{K})\mathrm{sgn}(\sigma) & \mathrm{u}\le\max\\ \mathrm{u(max)} & \mathrm{u}>\max\end{cases}\end{aligned} \tag{39}$$

With the constant K deleted, $\dot{\sigma}$ is represented by $\Theta(\eta,\upsilon,t)$, where $\dot{\widehat{\hbar}}$ is set to the following value:

$$\dot{\widehat{\hbar}}=-\frac{\Theta(\eta,\upsilon,t)}{\partial\widetilde{\hbar}}|s| \tag{40}$$

Computing the time derivative of Eq. (34), we obtain

$$\begin{aligned}\dot{V}&=\sigma\dot{\sigma}+\partial\widetilde{\hbar}\dot{\widetilde{\hbar}}\\&=\sigma\left(\Lambda u+\vartheta(\eta,\upsilon)+\wp(\eta,\upsilon,t)-\ddot{x}_d+\lambda\dot{e}\right)+\partial(\hbar-\widehat{\hbar})\dot{\widehat{\hbar}}\\&=\begin{cases}\sigma\left(\Lambda\left(\Lambda^{-1}\left(-\vartheta(\eta,\upsilon)+\ddot{x}_d\right)+\xi(\eta,\upsilon,t)-(\varepsilon+\widehat{\hbar}+\mathrm{K})\mathrm{sgn}(\sigma)\right)+\vartheta(\eta,\upsilon)+\wp(\eta,\upsilon,t)-\ddot{x}_d+\lambda\dot{e}\right)+\partial(\hbar-\widehat{\hbar})\dot{\widehat{\hbar}} & \mathrm{u}\le\max\\ \sigma\left(\Lambda u(\max)+\vartheta(\eta,\upsilon)+\wp(\eta,\upsilon,t)-\ddot{x}_d+\lambda\dot{e}\right)+\partial(\hbar-\widehat{\hbar})\dot{\widehat{\hbar}} & u>\max\end{cases}\\&=\begin{cases}\sigma\left(\Lambda\left(\Lambda^{-1}\left(-\vartheta(\eta,\upsilon)+\ddot{x}_d\right)+\xi(\eta,\upsilon,t)-(\varepsilon+\widehat{\hbar}+\mathrm{K})\mathrm{sgn}(\sigma)\right)+\vartheta(\eta,\upsilon)+(u_s+\delta)-\ddot{x}_d+\lambda\dot{e}\right)+\partial(\hbar-\widehat{\hbar})\dot{\widehat{\hbar}} & \mathrm{u}\le\max\\ \sigma\left(\Lambda u(\max)+\vartheta(\eta,\upsilon)+(u_s+\delta)-\ddot{x}_d+\lambda\dot{e}\right)+\partial(\hbar-\widehat{\hbar})\dot{\widehat{\hbar}} & u>\max\end{cases}\end{aligned} \tag{41}$$

Combining system Eqs. (34)–(39) and substituting them in Eq. (41), we obtain

$$\begin{aligned}\dot{V}&=\sigma\left(\Lambda u+\vartheta(\eta,\upsilon)+(-(\widehat{\hbar}+\mathrm{K})\mathrm{sgn}(\sigma)+\delta)-\ddot{x}_d+\lambda\dot{e}\right)+\partial(\hbar-\widehat{\hbar})\dot{\widehat{\hbar}}\\&=\sigma((-(\widehat{\hbar}+\mathrm{K})\mathrm{sgn}(\sigma)+\delta)-(\hbar-\widehat{\hbar})|\sigma|\\&\le-\mathrm{K}|\sigma|\\&\le0\end{aligned} \tag{42}$$

where K is a positive constant, $\dot{V}$ is strictly negative, and the entire system gradually becomes stable. In actual operation, the output of the controller is always less than the threshold, so the above formula is established, and the controller is always stable.

4. Simulation results

In order to demonstrate the effectiveness of the proposed SMC unified with the UDE control scheme, a simulation experiment of vessel based on the Matlab/Simulink environment was conducted. The supply vessel in (Fossen et al., 1996) was considered as the object for the simulation experiment in this study; the length of this vessel is 76.2 m,

and its mass is 4591 tons. The parameter matrices M, $C(\upsilon)$, and D are expressed as follows:

$$M = 10^6 \times \begin{bmatrix} 5.3122 & 0 & 0 \\ 0 & 8.2831 & 0 \\ 0 & 0 & 3745.4 \end{bmatrix}$$

$$C(\upsilon) = 10^6 \times \begin{bmatrix} 0 & 0 & 8.2831v \\ 0 & 0 & 5.3122u \\ 8.2831v & -5.3122u & 0 \end{bmatrix}$$

$$D = 10^4 \times \begin{bmatrix} 5.0242 & 0 & 0 \\ 0 & 27.299 & -439.33 \\ 0 & -439.33 & 41894 \end{bmatrix}$$

The first-order Markov process is used to describe the external disturbance of the DP vessel (Du et al., 2015):

$$d = J^T(\phi)b \tag{43}$$

$$\dot{b} = -T_c^{-1}b + pn \tag{44}$$

where $b \in R^3$ is the external environmental interference acting on the DP vessel in the inertial coordinate system of the Earth. $T_c = diag(10^3, 10^3, 10^3)$ is the selected time constant diagonal matrix; $p = 10^5 \times diag(5, 5, 50)$ is the amplitude matrix of n; and $n \in R^3$ is a zero-mean Gaussian white noise vector.

The driving force and torque are specified in the following range (Shen et al., 2020):$\tau_1 \in [-8 \times 10^3, 1 \times 10^4](KN)$, $\tau_2 \in [-1 \times 10^5, 2.5 \times 10^4](KN)$, $\tau_3 \in [-4 \times 10^5, 1.5 \times 10^5](KN \quad m)$.

The following parameters are used to simulate the uncertainty in the parameters of the DP vessel:

$$\Delta M = 10^6 \times \begin{bmatrix} 0.1 & 0 & 0 \\ 0 & 0.1 & 0 \\ 0 & 0 & 0.1 \end{bmatrix}$$

$$\Delta D = 10^7 \times \begin{bmatrix} 0.0001 & 0 & 0 \\ 0 & 0.0001 & 0.0001 \\ 0 & 0.0001 & 1 \end{bmatrix}$$

In this study, for designing the SMC unified with the UDE for a three-degree-of-freedom DP vessel, $G_f(s)$ is set as $\frac{1}{50s^2+5s+1}$, $\partial(\eta, \upsilon, t)$ is set as $10^6 \times diag(1, 1, 10^3)$, λandε is set as 1×10^{-4} The parameters of SMC are firstly chosen from Ref. (Shen, 2019) and then determined by trial and error. Ref. (Shen et al., 2020) is used as a reference for the parameters of the neural network observer. During the actual simulation, two cases are considered for the DP vessel: straight-line trajectory tracking and curve trajectory tracking. At the end of the paper, the operation of the three controllers under complex conditions is shown. First, the performances of the DP vessel controllers for straight-line trajectory tracking are tested. Simultaneously, the proposed SMC unified with the UDE is compared with the SMC based on the neural network observer (NN-based SMC) and the traditional SMC controller. The simulation results thus obtained are presented in Figs. 3–30.

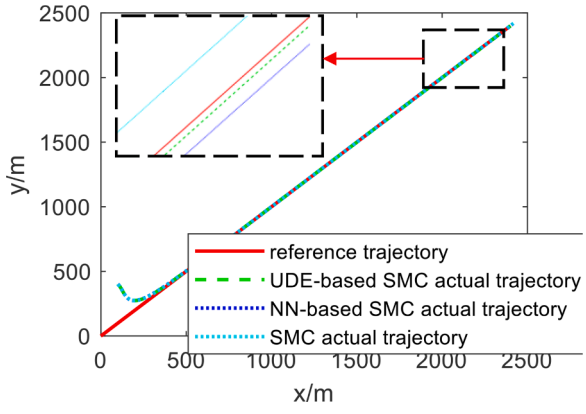

Fig. 3. Trajectory of ship's motion.

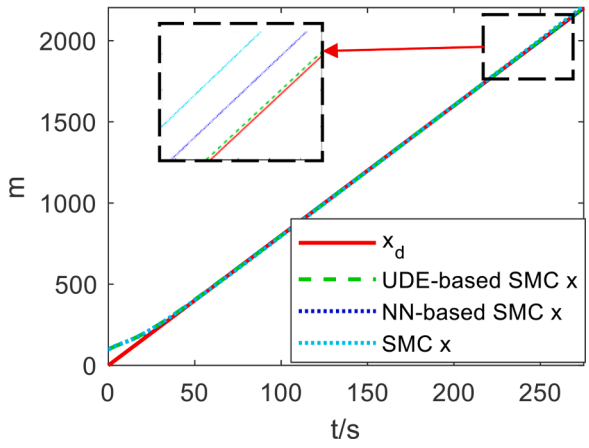

Fig. 4. North position of ship's motion.

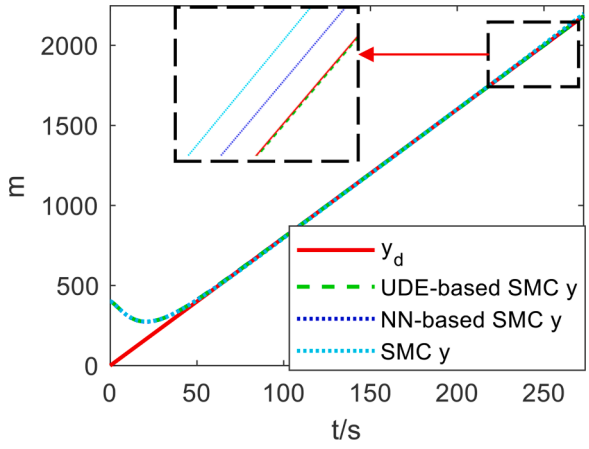

Fig. 5. East position of ship's motion.

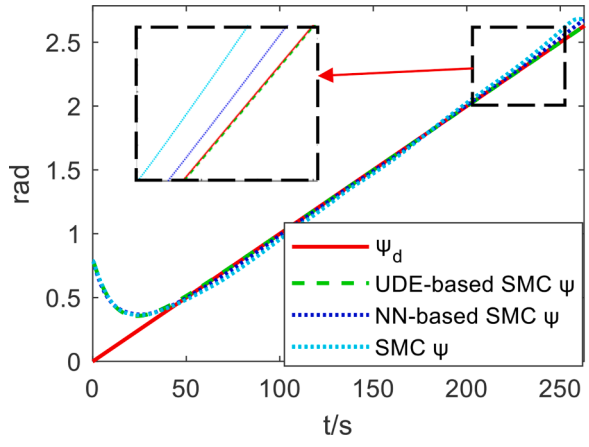

Fig. 6. Heading of ship's motion.

The straight-line trajectory tracking results are presented in Figs. 3–16; the linear trajectory is expressed as $x_d = 8t, y_d = 8t$, and $\phi_d = 0.01t$. The initial position of the vessel is $[x(0) \quad y(0) \quad \phi(0) \quad u(0) \quad v(0) \quad r(0)]^T = \left[100 \quad 400 \quad \frac{\pi}{4} \quad 0 \quad 0 \quad 0\right]^T$,

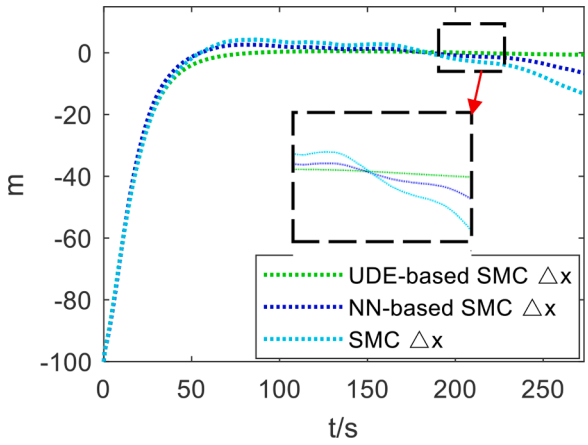

Fig. 7. Difference in north positions.

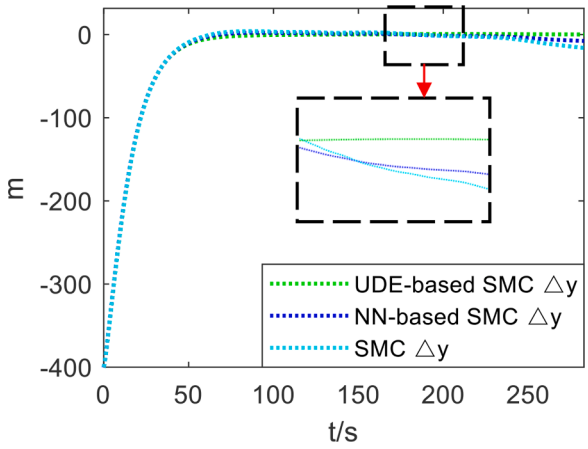

Fig. 8. Difference in east positions.

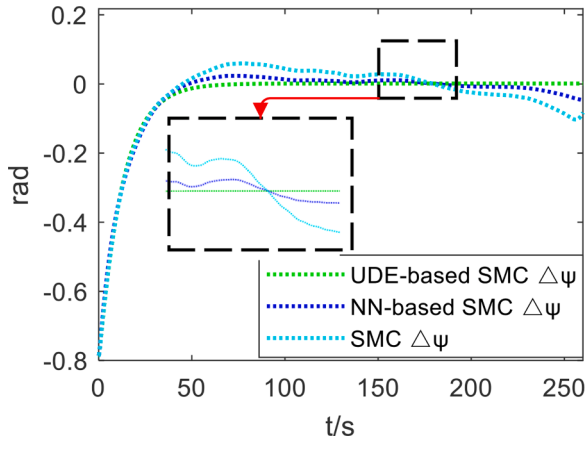

Fig. 9. Difference in headings.

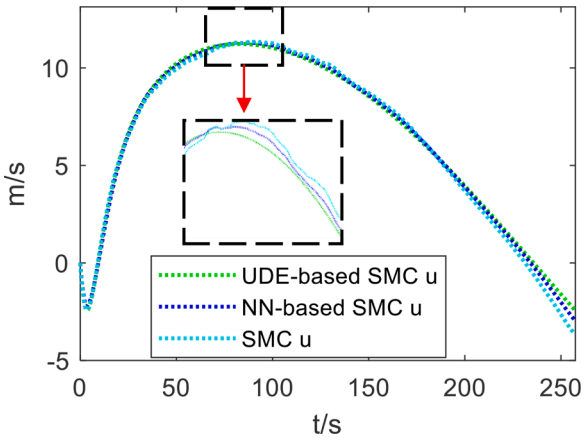

Fig. 10. Surge velocity of ship's motion.

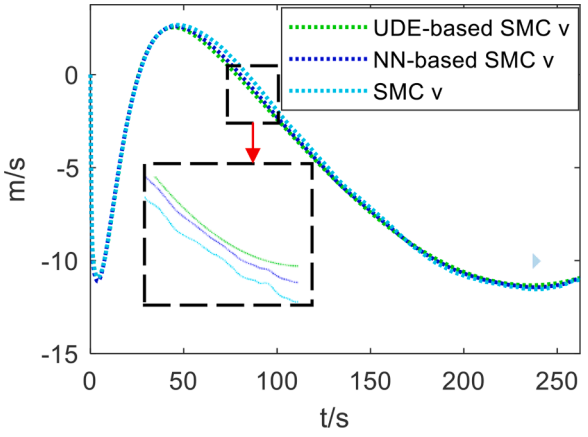

Fig. 11. Sway velocity of ship's motion.

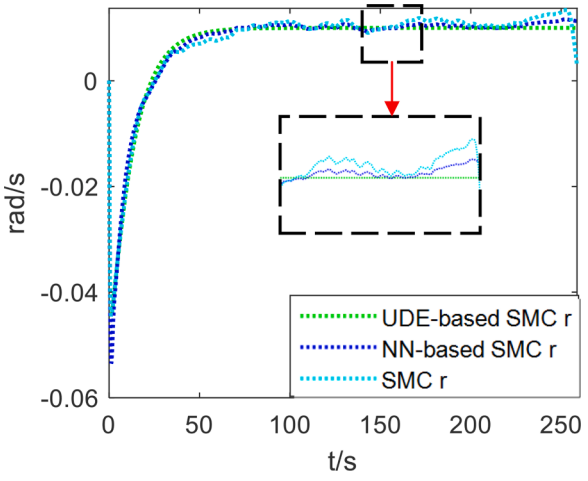

Fig. 12. Yaw rate of ship's motion.

which represents the control effect of the DP vessel when it travels along a straight path.

The expected linear trajectory of the DP vessel in an inertial coordinate system and the actual trajectory of the DP vessel actuate based on three types of control laws, as shown in Fig. 3; this indicates that the SMC unified with the UDE performs well for straight-line trajectory tracking under modelling uncertainties and disturbances. The time curves of the desired trajectory and the actual trajectory are shown in Figs. 4 and 5. It can be seen that the tracking trace of conventional SMC exhibits a relatively large deviation after approximately 250 *s*, and the control effect of NN-based SMC is between traditional SMC and UDE-based SMC. Based on the partially enlarged view, it can be deduced that the SMC unified with the UDE achieves better accuracy in trajectory tracking. The actual and desired headings for the SMC unified with the UDE, conventional SMC and NN-based SMC are shown in Fig. 6. It is evident that the SMC unified with the UDE achieves better tracking of the vessel's heading. The position and heading differences between the

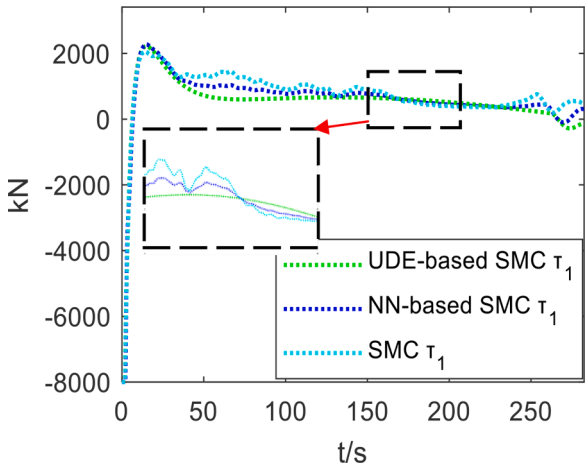

Fig. 13. Surge control force τ_1

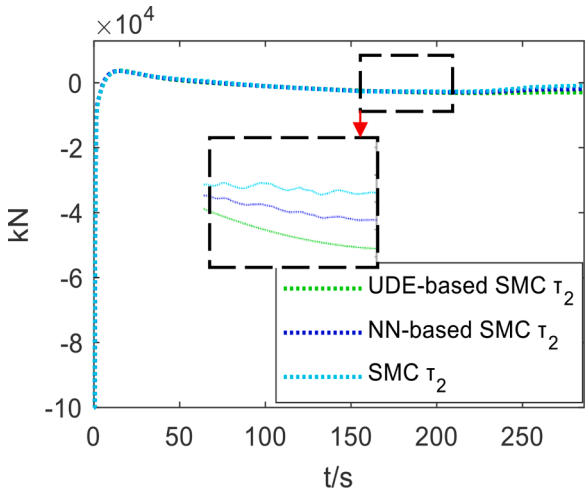

Fig. 14. Sway control force τ_2

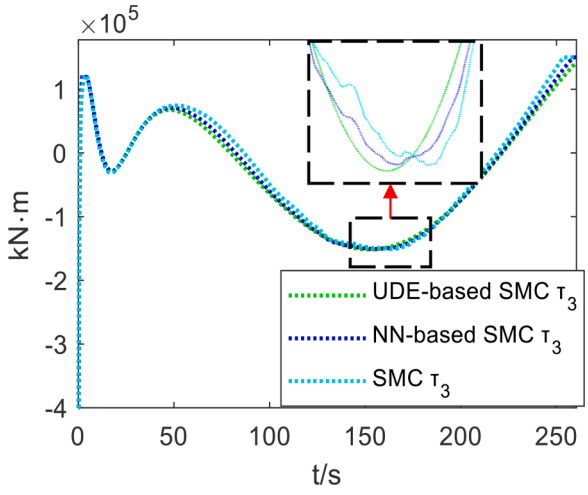

Fig. 15. Yaw moment τ_3.

three control methods and the required trajectory are presented in Figs. 7–9; these provide a more intuitive representation of the control performance of the SMC unified with the UDE. The duration curves of surge velocity, sway velocity, and yaw rate for the three control modes

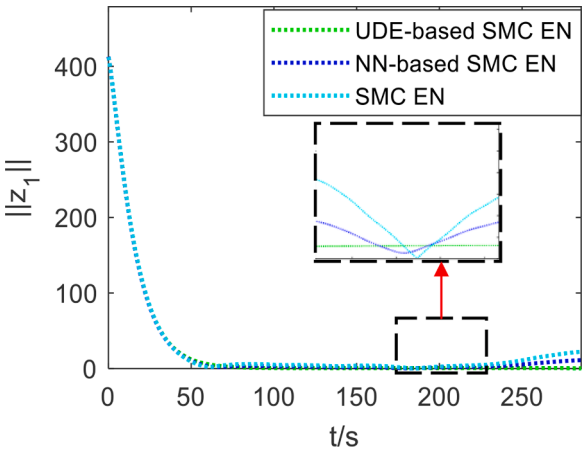

Fig. 16. Tracking performance of ship's motion.

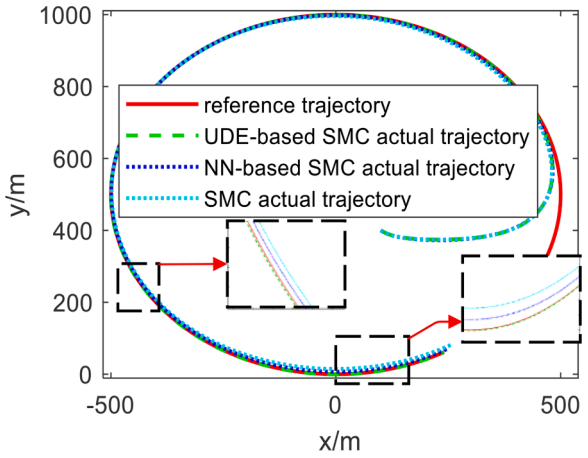

Fig. 17. Trajectory of ship's motion.

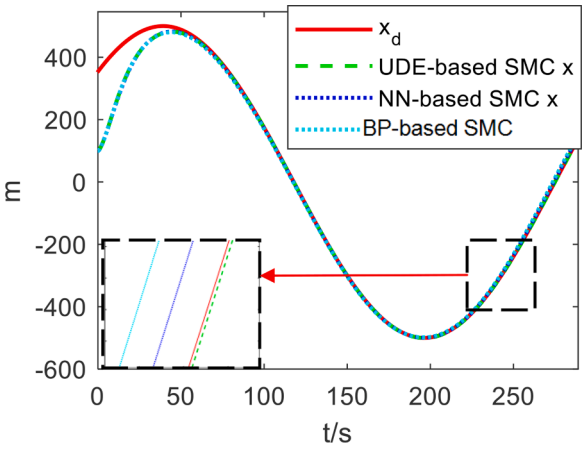

Fig. 18. North position of ship's motion.

under uncertain modelling and unknown disturbances are presented in Figs. 10–12. SMC unified with the UDE features reduced chattering, making it more suitable for practical engineering applications. The control output of the three control modes are depicted in Figs. 13-15. In actual operation, the DP ship's thruster output will have a threshold limit, thus the maximum output of the controller is also limited in the simulation. It can be seen that the control of the SMC unified with the UDE is more stable and without chattering. Compared with the

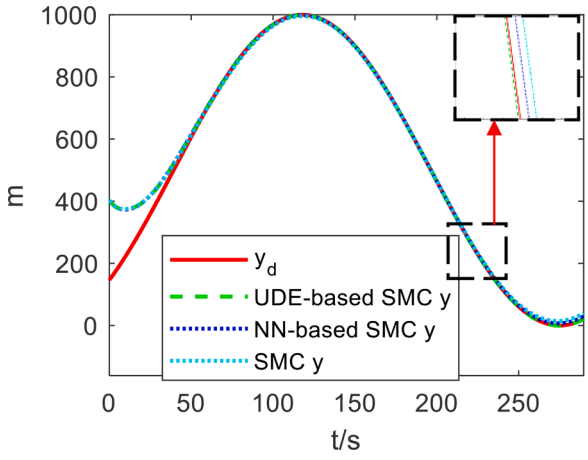

Fig. 19. East position of ship's motion.

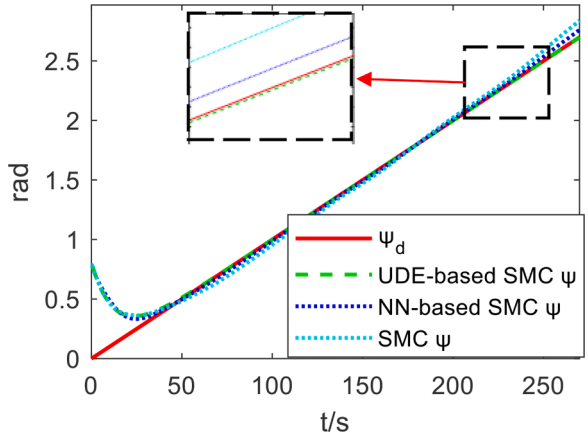

Fig. 20. Heading of ship's motion.

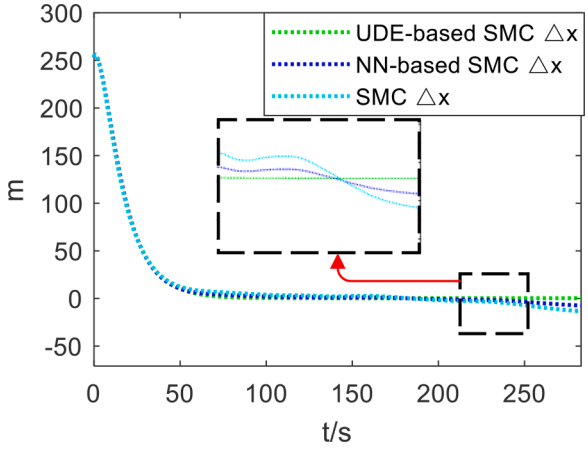

Fig. 21. Difference in north positions.

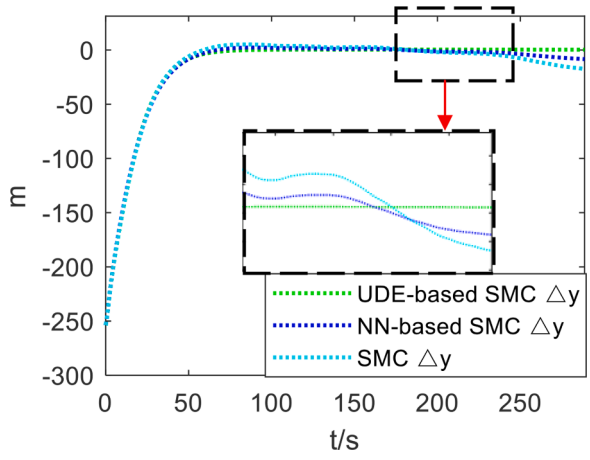

Fig. 22. Difference in east positions.

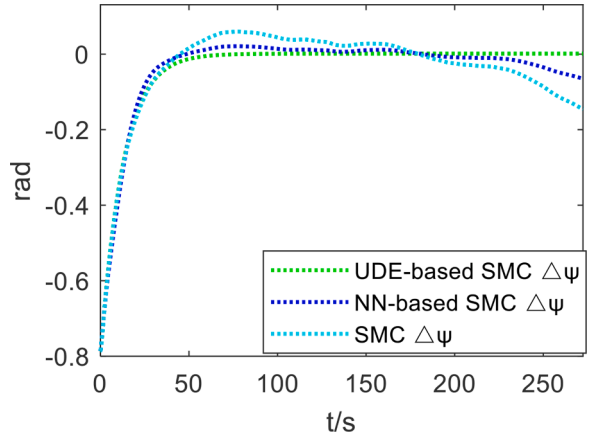

Fig. 23. Difference in headings.

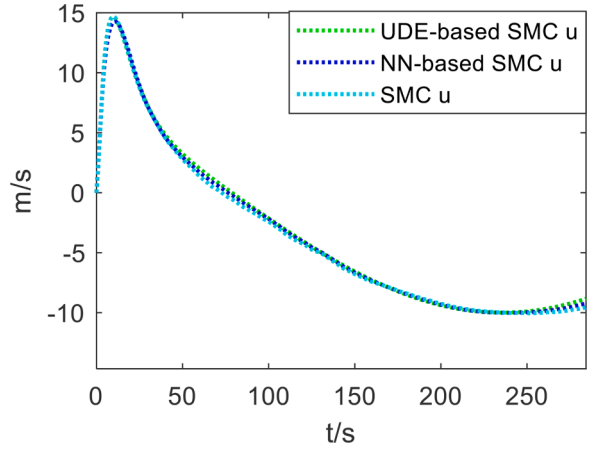

Fig. 24. Surge velocity of ship's motion.

conventional SMC and NN-based SMC, the proposed method has a smoother trajectory without chattering. The positions errors in linear trajectory tracking for the UDE-based SMC, NN-based SMC and the conventional SMC are demonstrated in Fig. 16, where the ordinate is $EN = \| \eta - \eta_d \|$. It is noted that the control performance of the UDE-based SMC is more stable when the modelling is uncertain.

The circular trajectory tracking of the DP vessel under uncertain modelling and unknown disturbances is presented in Figs. 17–30. The circular trajectory is expressed as $x_d = 500\sin\left(0.02t + \frac{\pi}{4}\right), y_d = 500\left[1 - \cos\left(0.02t + \frac{\pi}{4}\right)\right]$, and $\phi_d = 0.01t$; the initial position of the vessel is $[x(0) \quad y(0) \quad \phi(0) \quad u(0) \quad v(0) \quad r(0)]^T = \left[100 \quad 400 \quad \frac{\pi}{4} \quad 0 \quad 0 \quad 0\right]^T$

Higher requirements for the controller are noted in the circular trajectory tracking. Similar to the straight-line trajectory tracking, the expected and actual trajectories for the three controllers of the DP vessel

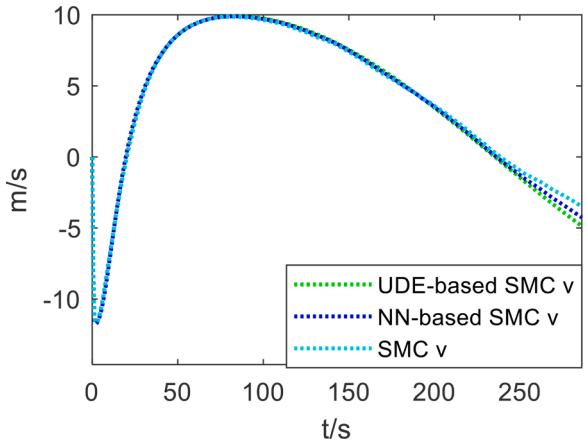

Fig. 25. Sway velocity of ship's motion.

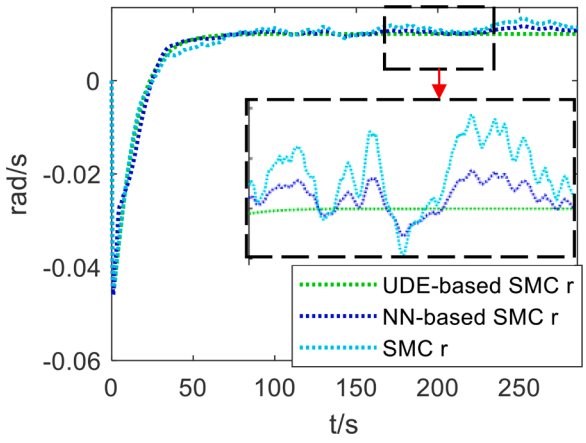

Fig. 26. Yaw rate of ship's motion.

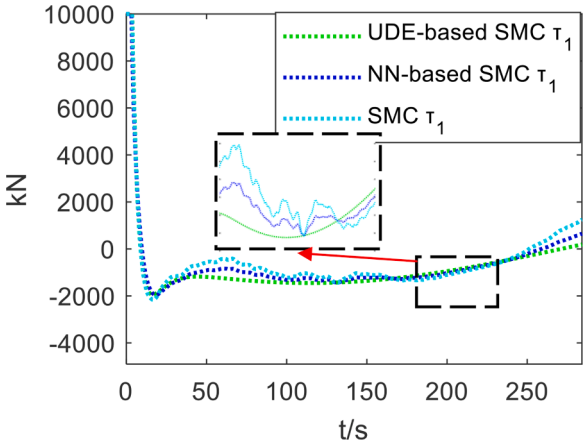

Fig. 27. Surge control force τ_1.

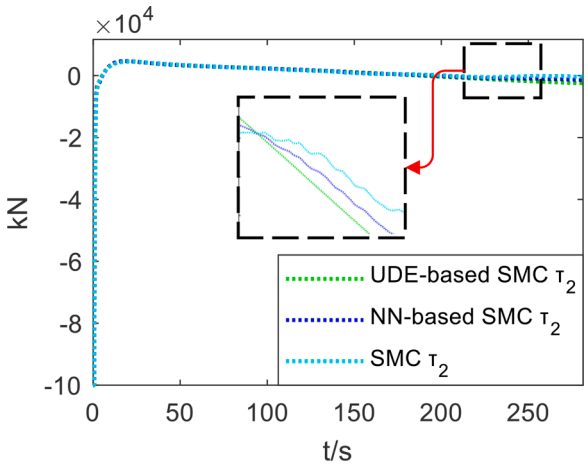

Fig. 28. Sway control force τ_2.

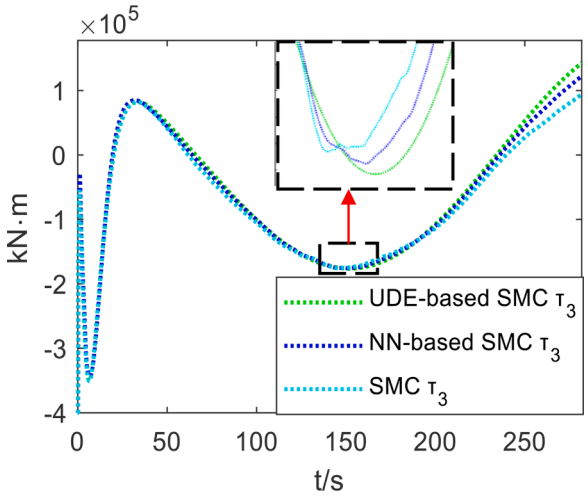

Fig. 29. Yaw moment τ_3.

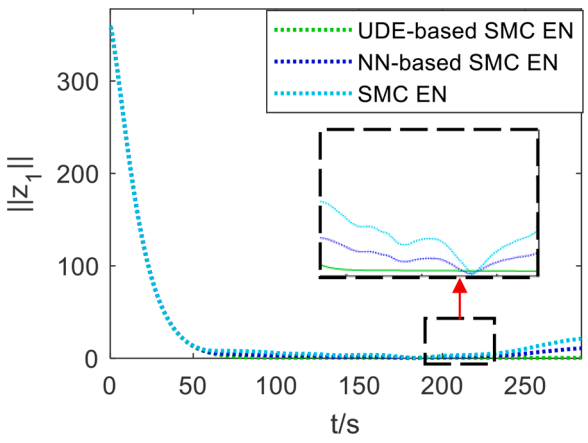

Fig. 30. Tracking performance of ship's motion.

are presented in Fig. 17. In the case of real-time changes in heading, the control performance of the SMC unified with the UDE is significantly better than that of the conventional SMC and NN-based SMC. Similar to straight-line trajectory tracking, time curves of the actual position and heading for the SMC unified with the UDE, NN-based SMC and the conventional SMC are depicted in Figs. 18–20. The differences in the positions and headings for the three control methods and the required trajectory are shown in Figs. 21–23; these provide a more intuitive representation of the control performance of the SMC unified with the UDE. The time curves of surge velocity, sway velocity, and yaw rate of the three control modes in the case of uncertain modelling and disturbances are shown in Figs. 24–26. The time curves of the control output for the three control modes are presented in Figs. 27–29. The position error during circular trajectory tracking is shown in Fig. 30. It can be seen from Figs. 17–30, the conventional SMC is significantly inadequate

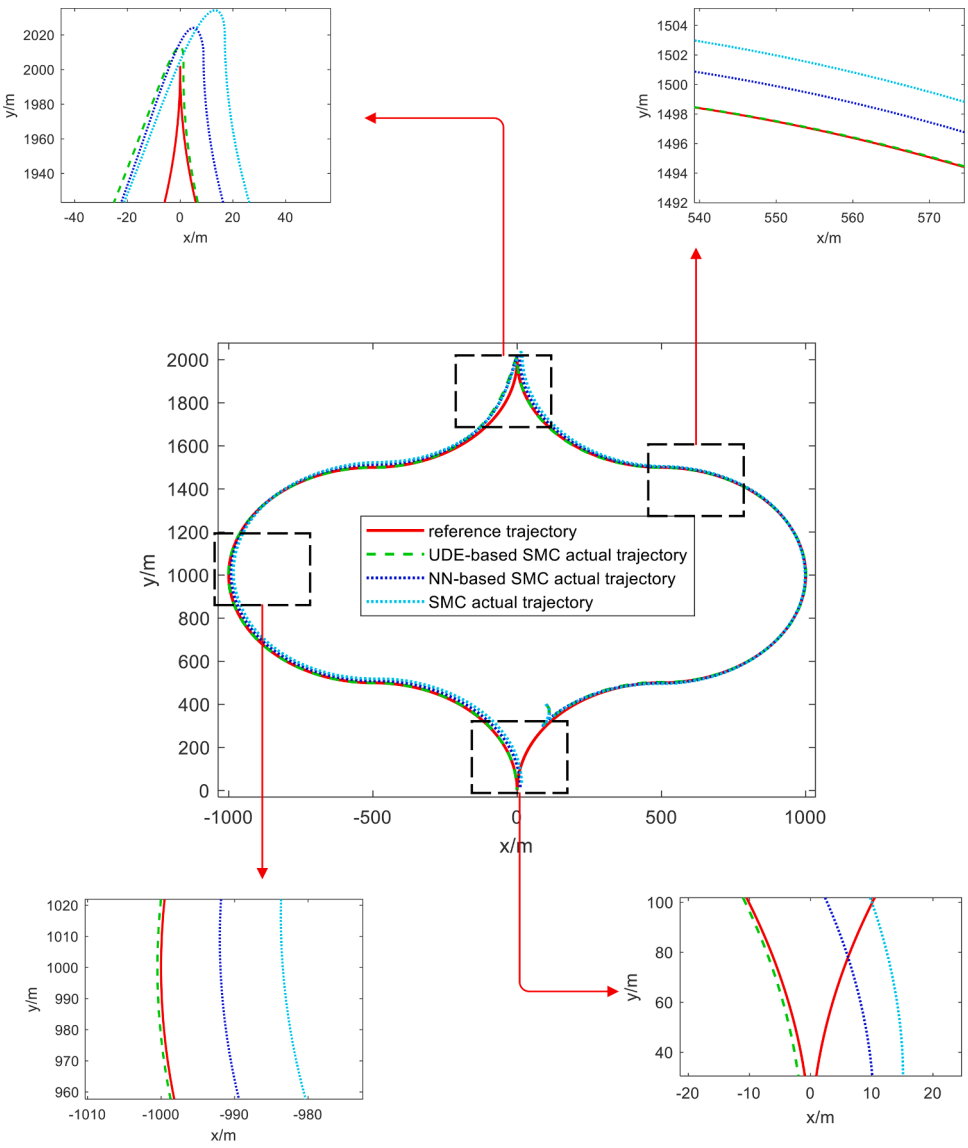

Fig. 31. The trajectory of the ship in complex trajectory.

for meeting the requirements of control accuracy when the heading in the circular trajectory changes considerably. The control performance of NN-based SMC is between conventional SMC and proposed control method, because NN-based SMC can observe the total uncertainty to a certain extent and be compensated in conventional SMC. The control performances of proposed control strategy are significantly better than conventional SMC and NN-based SMC.

The effect of SMC unified with the UDE in complex trajectories is also very satisfactory, as can be seen from Fig. 31.

5. Conclusions

This paper proposes a novel control strategy involving SMC unified with the UDE; this proposed strategy combines modelling uncertainty and unknown disturbances into the total uncertainty. This total uncertainty is then observed using the UDE and compensated via SMC. Finally, a good trajectory tracking performance is obtained, accompanied with a higher accuracy in the trajectory tracking of a DP vessel. Simulations are used to validate and highlight the effectiveness of the proposed control scheme. The control strategies of DP ship are simulated and operated in two common trajectories and a comprehensive complex trajectory, and the threshold of the ship's thruster is taken into consideration. The control effects of SMC unified with the UDE, NN-based SMC and conventional SMC are compared. The experimental results prove the proposed control strategy can effectively eliminate the chattering of traditional sliding mode control and improve the control accuracy.

CRediT authorship contribution statement

Chaodong Hu: Writing – original draft, Writing – review & editing. **Defeng Wu:** Writing – review & editing, Supervision, Funding acquisition. **Yuxiang Liao:** Validation. **Xin Hu:** Supervision.

Declaration of Competing Interest

The authors declare that they have no conflict of interest.

Acknowledgments

This study was financially supported by the National Natural Science Foundation of China (51809113, 51249006), the Fujian Province Science and Technology Department (2019H0019), the Fujian Education Department (FBJG20180056, JT180266), and the Fujian Provincial

Young Top-Notch Talent Plan (Z02101) .

References

Aharon., I., Shmilovitz, D., Kuperman., A., 2011. Uncertainty and disturbance estimator-based controllers under finite control bandwidth constraint. Int. J. Roubust Nonlinear Control 21 (1), 79–92.

Basin, M.V, Yu, P, Shtessel, Y.B, Y.B, 2017. Hypersonic missile adaptive sliding mode control using finite and fixed-time observers. IEEE Trans. Ind. Electron. 65 (1), 930–941.

Chen, Y., Yu, S., Huang, J., Li, C., Lin, Z., 2016. Cooperative tracking of marine vessel based on sliding mode. In: 2016 Chinese Control and Decision Conference (CCDC), pp. 1372–1376.

Chen, Z., Huang, F., Chen, W., Zhang, J., Sun, W., Chen, J., Gu, J., Zhu, S., 2020. RBFNN-based adaptive sliding mode control design for delayed nonlinear multilateral telerobotic system with cooperative manipulation. IEEE Trans. Ind. Inf. 16 (Feb.(2)), 1236–1247.

Chen, Z., Huang, F., Sun, W., Gu, J., Yao, B., 2020. RBF-neural-network-based adaptive robust control for nonlinear bilateral teleoperation manipulators with uncertainty and time delay. IEEE/ASME Trans. Mechatron. 25 (2), 906–918.

Deepika, D., Sandeep, K., Shiv, N., 2018. Uncertainty and disturbance estimatorbased robust synchronization for a class of uncertain fractional chaotic system via fractional order sliding mode control. Chaos Solitons Fractals 115, 196–203.

Hadi, D., Hamid, H., Heydarinejad, H., 2018. Fractional-order backstepping sliding-mode control based on fractional-order nonlinear disturbance observer. J. Comput. Nonlinear Dynam. 13 (11), 111–119.

Du, J., Hu, X., Liu, H., Chen, C.L.P., 2015. Adaptive robust output feedback control for a marine dynamic positioning system based on a high-gain observer. IEEE Trans. Neural Netw. Learn. Syst. 26 (11), 2775–2786.

Fahimi, F., 2007. Sliding-mode formation control for underactuated surface vessel. IEEE Trans. Robot. 23 (3), 617–622.

Fossen, T.I., Strand, J.P., 1999. Passive nonlinear observer design for ships using Lyapunov methods: full-scale experiments with a supply vessel. Automatica 35, 3–16.

Fu, M., Yu, L., 2018. Finite-time extended state observer-based distributed formation control for marine surface vehicles with input saturation and disturbances. Ocean Eng. 159, 219–227.

Gadelovits, S.Y., Zhong, Q.C., Kadirkamanathan, V., Kuperman, A., 2017. UDE-based controller equipped with a multi-band-stop filter to improve the voltage quality of inverters. IEEE Trans. Ind. Electron. 64 (9), 7433–7443.

Hu, R., Deng, H., Zhang, Y., 2020. Novel dynamic-sliding-mode-manifold-based continuous fractional-order nonsingular terminal sliding mode control for a class of second-order nonlinear systems. IEEE Access 8, 19820–19829.

Fossen, T., Sagatun, S., Srensen, A., 1996. Identification of dynamically positioned ships. Model. Identif. Control 17 (2), 369–376.

Kim, G., Hong, K., 2019. Adaptive sliding-mode control of an offshore container crane with unknown disturbances. IEEE/ASME Trans. Mechatron. 24 (6), 2850–2861.

An, L., Li, Y., Jiang, Y., Li, Y., Cao, J., He, J., Yueming, L., Jian, C., Jiayu, H., 2019. Soft-switching proximate time optimal heading control for underactuated autonomous underwater vehicle. IEEE Access 7, 143233–143249.

Liu, M., Zhang, L., Shi, P., Karimi, H.R., 2014. Robust control of stochastic systems against bounded disturbances with application to flight control. IEEE Trans. Ind. Electron. 61 (3), 1504–1515.

Ma, X., Guo, Y., Chen, L., 2018. Active disturbance rejection control for electric power steering system with assist motor variable mode. J. Franklin Inst. 355 (3), 1139–1155.

Qin, J., Ma, Q., Gao, H., Zheng, W.X., 2018. Fault-tolerant cooperative tracking control via integral sliding mode control technique. IEEE/ASME Trans. Mechatron. 23 (1), 342–351.

Ren, B., Zhong, Q., Chen, J., 2015. Robust control for a class of nonaffine nonlinear systems based on the uncertainty and disturbance estimator. IEEE Trans. Ind. Electron. 62 (9), 5881–5888.

Sanz, R., García, P., Zhong, Q., Albertos, P., 2017. Predictor-based control of a class of time-delay systems and its application to quadrotors. IEEE Trans. Ind. Electron. 64 (1), 459–469.

Shen, Z., 2019. Ship Motion Adaptive Sliding Control [M]. Science Press, Beijing.

Shen, Z., Bi, Y., Wang, Y., Guo, C., 2020. MLP neural network-based recursive sliding mode dynamic surface control for trajectory tracking of fully actuated surface vessel subject to unknown dynamics and input saturation. Neurocomputing 377, 103–112.

Shen, Z., Wang, Y., Yu, H., Guo, C., 2020. Finite-time adaptive tracking control of marine vehicles with complex unknowns and input saturation. Ocean Eng. 198.

Tian, Z., Zhong, Q., Ren, B., Yuan, J., 2019. Stabilisability analysis and design of UDE-based robust control. IET Control Theory Appl. 13 (10), 1445–1453.

Verma, B., Padhy, P.K., 2020. Robust fine tuning of optimal PID controller with guaranteed robustness. IEEE Trans. Ind. Electron. 67 (6), 4911–4920.

Wang, D., Liu, S., Zhang, X., Tang, Q., 2014. A novel backstepping sliding mode dynamic surface control. In: Proceeding of the 11th World Congress on Intelligent Control and Automation, pp. 4778–4783.

Wang, L., Wang, W., Du, Y., Huang, Y., 2019. A novel adaptive fuzzy PID controller based on piecewise PID controller for dynamic positioning of sandglass-type FDPSO. J. Mar. Sci. Technol. 24, 720–737.

Wu, D., Liao, Y., Hu, C., Yu, S., Tian, Q., 2021. An enhanced fuzzy control strategy for low-level thrusters in marine dynamic positioning systems based on chaotic random distribution harmony search. Int. J. Fuzzy Syst. https://doi.org/10.1007/s40815-020-00989-5.

Wu, D., Liu, X., Ren, F., Yin, Z., 2017. An improved thrust allocation method for marine dynamic positioning system. Naval Eng. J. 129 (3), 89–98.

Huang, Y., Wu, D., Yin, Z., Yuan, Z., 2021. Design of UDE-based dynamic surface control for dynamic positioning of vessels with complex disturbances and input constraints. Ocean Eng. 220, 216–226.

Wu, D., Ren, F., Zhang, W., 2016. An energy optimal thrust allocation method for the marine dynamic positioning system based on adaptive hybrid artificial bee colony algorithm. Ocean Eng. 118, 216–226.

Wu, Y., Li, G., 2018. Adaptive disturbance compensation finite control set optimal control for PMSM systems based on sliding mode extended state observer. Mech. Syst. Signal Process. 98 (1), 402–414.

Xie, W., Liu, B., Bu, L., Wang, Y., Zhang, J., 2021. A decoupling approach for observer-based controller design of T-S fuzzy system with unknown premise variables. IEEE Trans. Fuzzy Syst. https://doi.org/10.1109/TFUZZ.2020.

Yu., S., Yu, X., Shirinzadeh, B., Man, Z., 2005. Continuous finite-time control for robotic manipulators with terminal sliding mode. Automatica 41, 1957–1964.

Zhang, Q., Zhang, J., Chemori, A., Xiang, X., 2018. Virtual submerged floating operational system for robotic manipulation. Complexity 2018, 18.

Yang, J., Hu, J., Lv, X., 2007. Design of sliding mode tracking control for hypersonic reentry vehicles. 2007 Chinese Control Conference 2–5.